Journal of Materials Chemistry A

RSC Publishing

COMMUNICATION

View Article Online
View Journal | View Issue

Cite this: J. Mater. Chem. A, 2013, 1, 515

Received 22nd August 2012
Accepted 6th November 2012

DOI: 10.1039/c2ta00025c

www.rsc.org/MaterialsA

Composite cathodes composed of $NdBa_{0.5}Sr_{0.5}Co_2O_{5+\delta}$ and $Ce_{0.9}Gd_{0.1}O_{1.95}$ for intermediate-temperature solid oxide fuel cells

Jiyoun Kim,[a] Won-yong Seo,[a] Jeeyoung Shin,[b] Meilin Liu[c] and Guntae Kim*[a]

The electrochemical properties of a composite cathode composed of $NdBa_{0.5}Sr_{0.5}Co_2O_{5+\delta}$ (NBSCO) and $Ce_{0.9}Gd_{0.1}O_{1.95}$ (GDC) are investigated for intermediate-temperature solid oxide fuel cells (IT-SOFCs). In particular, cells based on NBSCO–GDC composite cathodes demonstrated higher performance than those based on a NBSCO cathode, probably due to the extended triple phase boundary (TPB) length. The oxygen reduction mechanism on the NBSCO–GDC composite cathodes is proposed to explain the superior electrochemical behaviour.

Introduction

Solid oxide fuel cells (SOFCs) convert chemical energy directly to electrical energy by means of electrochemical oxidation of various fuels, with high efficiency and low emissions. The conventional operating temperatures above 1073 K pose many problems, such as chemical reactions and mismatch in thermal expansion between cell components, which impose severe limitations on the choice of electrode and interconnector materials. Significant efforts, therefore, have focused on lowering the operation temperature to enhance long-term stability and reduce the costs.[1,2] It is essential to attain high electrochemical activity in the cathode for intermediate temperature applications, because the polarization loss of the cathode at intermediate-temperatures is a limiting factor to cell performance.[3,4]

In this regard, cation ordered perovskite-related oxides, such as $LnBaCo_2O_{5+\delta}$ (Ln = Pr, Nd, Sm, Gd and Y), have recently been recognized as one of the best cathode materials for intermediate-temperature (IT) SOFCs, owing to their substantially high electrical conductivities, rapid oxygen exchange, and fast oxygen diffusion characteristics.[4,5]

The crystals of $LnBaCo_2O_{5+\delta}$ (Ln = Nd, Sm, and Gd) have Ln–O and Ba–O layers alternating along the *c*-axis, where the difference in the ionic radii between the Ln^{3+} and Ba^{2+} ions plays a dominant role in determining the oxygen stoichiometry and the crystal structure.[6,7] For example, the oxygen content increases from 5.57 (Ln = Gd) to 5.78 (Ln = Nd) with increasing lanthanide ionic radius, as the crystal structure changes from an orthorhombic (Ln = Gd) to a tetragonal lattice (Ln = Nd). They exhibit high electrical conductivity, reasonable oxygen non-stoichiometry, and good cell performance.[8] Kim *et al.* reported that $PrBaCo_2O_{5+\delta}$ (PBCO) is a promising material for IT-SOFC cathodes, as it showed unusually fast oxygen kinetics at lower temperatures (773 to 973 K), resulting in low cathodic polarization.[9] Taskin *et al.* proposed that the formation of a layered crystal structure, with disorder-free channels for ion migration and with a weakened bonding strength of oxygen, can significantly facilitate oxygen motion through the crystal lattice, resulting in fast kinetics for $GdBaCo_2O_{5+\delta}$.[10]

Meanwhile, substitution of Sr^{2+} for Ba^{2+} may improve the electrochemical characteristics of cathode materials due to higher electrical conductivity and oxygen content followed by the smaller size difference between Ln^{3+} and Sr^{2+}. The substitution of Ba^{2+} by Sr^{2+} in $GdBaCo_2O_{5+\delta}$, for example, increases the oxygen content from 5.6 to 6.0; the corresponding increase of the oxygen content will increase the concentration of Co^{4+}, an electronic mobile species, leading to higher electrical conductivity.[6,11,12] In addition, when the crystal structure changes from an orthorhombic (*Pmmm*) to a tetragonal lattice (*P*4/*mmm*) with an increase of Sr^{2+}, the O–Co–O bond angle is also straightened toward the ideal value of 180°, leading to an increase in bandwidth and the covalency of the Co–O bond.[13,14] This is another reason for higher electrical conductivity with higher Sr^{2+} amounts.

It has been widely documented that a specific amount of secondary phase within cathode materials can be used as an electrocatalyst for optimized performance of the cathode. In particular, ceria based oxides such as $Ce_{0.9}Gd_{0.1}O_{1.95}$ (GDC) can improve the electrocatalytic activity of the cathode when they form a composite

[a]*Interdisciplinary School of Green Energy, KIER-UNIST Advanced Center for Energy, Ulsan National Institute of Science and Technology (UNIST), Ulsan, 689-798, Korea. E-mail: gtkim@unist.ac.kr; Fax: +82 52 217 2909; Tel: +82 52 217 2959*

[b]*Department of Mechanical Engineering, Dong-Eui University, 995 Eomgwangno, Busan-jin-gu, Busan, 614-714, Korea*

[c]*School of Materials Science and Engineering, Georgia Institute of Technology, 771 Ferst Drive, N.W., Atlanta, GA, 30332-0245, USA*

with the cathode material due to possible extension of the electrochemically active area, such as the triple phase boundary (TPB) where the electrochemical reaction occurs.[15]

The improved performance of the $NdBa_{0.5}Sr_{0.5}Co_2O_{5+\delta}$ (NBSCO)–*x*GDC (*x* = 0, 20, 40, and 50 wt%) composite cathode can be explained as follows: first, GDC and NBSCO are compatible both physically and chemically so that there is minimum reaction at the interface between the two phases. Second, the mismatch in thermal expansion between the two phases is also minimal, leading to better connectivity between the two phases.[16] Third, the mixture of GDC and NBSCO may create more TPB, the active sites for oxygen reduction.[17]

Schematically illustrated in Fig. 1 are the possible reaction zones for oxygen reduction reaction (ORR) on electrodes with different degrees of mixed-conductions, a traditional porous electronic conductor (Fig. 1a), a typical porous MIEC (Fig. 1b), and a MIEC–GDC composite cathode (Fig. 1c). When an electronic conducting material such as (La, Sr) MnO_3 (LSM) is used as the cathode, the ORR is largely confined to the electrode–electrolyte interface (TPB), where oxygen gas has synchronous access to both the electronically and ionically conductive phases (Fig. 1a, path ①).[18] When an MIEC is used as the cathode, however, the entire surface may serve as the active sites for ORR, because oxygen anions can transport through the MIEC bulk, *e.g.* $La_{0.6}Sr_{0.4}Co_{0.2}Fe_{0.8}O_{3-\delta}$ (Fig. 1b, path ②).[19] The electrochemically active region can be extended, because the ORRs can also take place on the two phase boundary (2PB) where the gas and mixed conductor meet.[17,20–31] Further, the combination of ionically conducting ceria with NBSCO may provide additional TPB sites for ORR (Fig. 1c, path ③). As illustrated in Fig. 1c, the reaction rate of the composite electrodes would be the sum of those on the 2PB sites (the surface of MIEC) and those on the TPB sites (all interface boundaries between NBSCO and GDC that are exposed to oxygen gas), which could be greater than the ORR sites of the electronic conductor or the MIECs.

In this study, we systematically varied the ratio of GDC to NBSCO in the two-phase composite cathodes in an effort to optimize the electrochemical properties under IT-SOFC operating conditions.

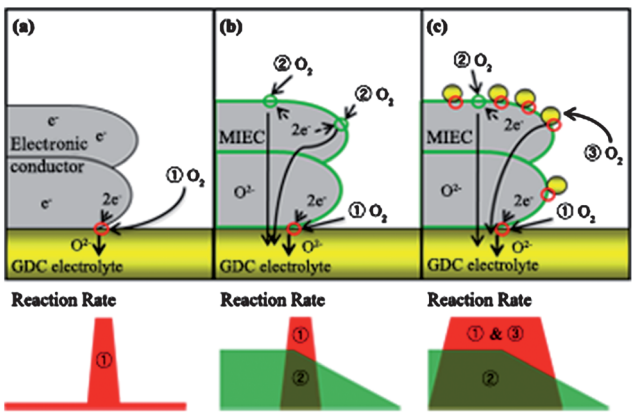

Fig. 1 Schematics of the oxygen reduction reaction at (a) electronic conductor (TPB concept), (b) MIEC (TPB + 2PB), and (c) MIEC-ionic conductor, GDC (enlarged TPB + 2PB) (path ①; TPB point between the electrolyte and cathode, path ②; 2PB point on the surface of NBSCO, and path ③; enhanced TPB point by addition of GDC).

Experimental

The NBSCO oxide was synthesized *via* the Pechini process. Metal nitrates are employed both as metal precursors and oxidizing agents. Stoichiometric amounts of $Nd(NO_3)_3 \cdot 6H_2O$ (Aldrich, 99.9%, metal basis), $Ba(NO_3)_2$ (Aldrich, 99+%), $Sr(NO_3)_2$ (Aldrich, 99+%), and $Co(NO_3)_2 \cdot 6H_2O$ (Aldrich, 98+%) were added into a beaker containing a suitable amount of concentrated nitric acid solution under continuous heating and stirring. An adequate amount of ethylene glycol was added into the beaker after the mixture was dissolved. After a viscous resin was formed, the mixture was heated around 473 K. The resultant products were pre-calcined at 873 K for 4 hours, ball-milled in acetone for 24 hours, and calcined at 1273 K for 12 hours in air.

The structure and morphology of the NBSCO were characterized by X-ray diffraction (XRD) and scanning electron microscopy (SEM). X-ray powder diffraction measurements (Rigaku diffractometer, Cu Ka radiation) were performed to confirm the structure with a scan rate of 0.5° min^{-1} and a range of $20° < 2\theta < 60°$. Chemical compatibility between NBSCO and GDC was evaluated by careful XRD analysis of an intimate mixture of 50 wt% NBSCO and 50 wt% GDC (NBSCO–50GDC) fired at high temperatures. An agate mortar and pestle were used to mix the fine NBSCO and GDC powders.

Glycine was applied to the solution at a molar ratio of 1 : 1.5 for metal nitrate and glycine. The electrode powders were blended with a binder (Heraeus V006) to form slurries for both symmetric and single cell fabrication. Electrochemical performances of the NBSCO–*x*GDC (*x* = 0, 20, 40, and 50 wt%) cathode were evaluated with Ni-GDC anode-supported single cells. To determine the optimized cell performance, the NBSCO powder and GDC were mixed at weight ratios of 10 : 0, 8 : 2, 6 : 4, and 5 : 5. The mixtures were ball-milled for 12 hours. The Ni-GDC cermet anode, thereafter, was fabricated from a mixture of nickel oxide, GDC prepared by GNP, and starch at a weight ratio of 6 : 4 : 1.5. This mixture was ball-milled in ethanol for 24 hours. The GDC powder electrolyte was pressed over the pelletized Ni-GDC cermet anode. The Ni-GDC/GDC anode-electrolyte layer was sintered at 1623 K for 5 hours. NBSCO–*x*GDC slurries were screen-printed on the GDC electrolyte as a cathode. The cells, with an active electrode area of 0.36 cm^2, were finally sintered at 1223 K for 4 hours in air. Ag wires were attached as a current collector to both the anode and cathode of a single cell using Ag paste. An alumina tube was employed to fix the single cell using a ceramic adhesive (Aremco, Cerama bond 553). H_2 containing 3% H_2O was supplied through a water bubbler with a flow rate of 20 mL min^{-1}, while ambient air was supplied as an oxidant to the cathode during the single cell test. A BioLogic Potentiostat was used to measure impedance spectra and *I–V* curves. Impedance Spectra Ware recorded the area specific resistance (ASR) under OCV conditions in a frequency range of 1 mHz to 500 kHz with an AC perturbation of 14 mA at 973 K. *I–V* polarization curves were measured between 773 K and 973 K.

Results

Chemical compatibility

XRD analysis was used to study the chemical compatibility between NBSCO and GDC. The NBSCO cathode material has a double

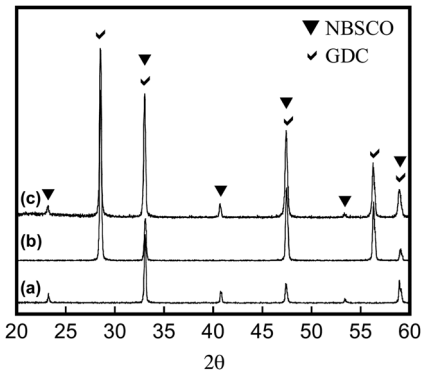

Fig. 2 XRD pattern of (a) NBSCO powder sintered at 1373 K for 12 hours, (b) $Ce_{0.9}Gd_{0.1}O_{1.95}$ (GDC) powder, and (c) NBSCO–GDC mixture sintered at 1273 K for 5 hours.

perovskite structure after being calcined at 1373 K for 12 hours, as implied by the XRD pattern shown in Fig. 2a. The characteristic diffraction peaks for the NBSCO sample suggest that it has a tetragonal structure without any detectable second phases.[32] The XRD pattern of a pure GDC sample is shown in Fig. 2b for comparison. The XRD pattern for a NBSCO–50GDC mixture fired at 1273 K for 5 hours is shown in Fig. 2c. Since all observable diffraction peaks correspond to those that are characteristic of the two components, NBSCO and GDC, the chemical compatibility between NBSCO and GDC is adequate under the processing condition.

SEM

The microstructures of the NBSCO–40GDC cathodes were examined under a SEM; typical micrographs are presented in Fig. 3. The thickness of the cathode is around 15–20 μm and it has a highly porous morphology that ensures good gas diffusion (Fig. 3a). The GDC electrolyte of 20 μm thick appears adhered well to the cathode and anode layers without any cracks, indicating good compatibility between the electrolyte and the electrode. Fig. 3c and d show that the GDC grains (small grains in the figure) are well deposited on the surface of the NBSCO backbone, as shown in Fig. 3b. It is clearly shown that additional TPB sites are developed with the mixture of the NBSCO backbone and small particles of GDC. With increasing amounts of GDC on NBSCO, more TPB sites can be formed, as shown as path ③ in Fig. 1c.

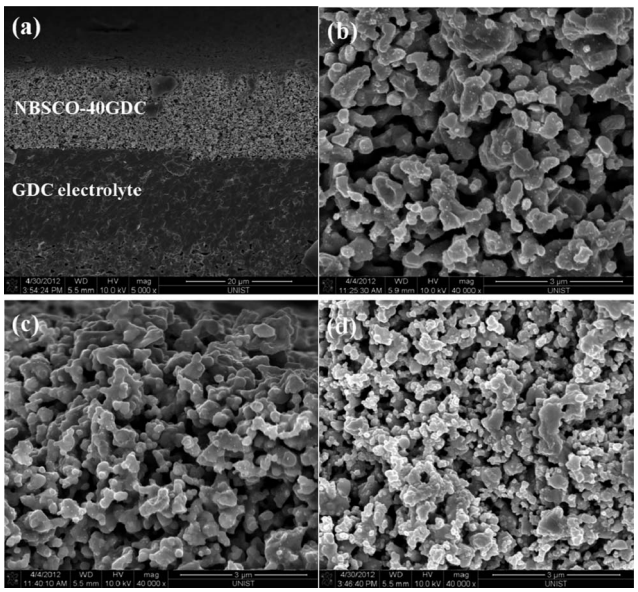

Fig. 3 SEM images of NBSCO–*x*GDC single cells, (a) NBSCO–40GDC single cell cross section, microstructure of (b) NBSCO–0GDC, (c) NBSCO–20GDC, and (d) NBSCO–40GDC composite cathode.

Electrochemical properties and performance

The area specific resistance (ASR) is used to describe all resistances associated with the electrode and electrolyte of the cell, including the gas–cathode interface, the bulk of the cathode, and the cathode–electrolyte interface. In a typical impedance spectrum, the intercept with the real axis at low frequency designates the total resistance of the cell and the intercept at high frequency is the ohmic resistance of the cell (mainly originated from the electrolyte). The magnitude of the semi-circle or the difference between the total resistance and the ohmic resistance is called the polarization resistance, and it is the total resistance to the cathodic processes associated with oxygen reduction reaction.

Fig. 4a shows the electrochemical impedance spectra of the NBSCO–GDC/GDC/NBSCO–GDC symmetric cells as a function of GDC content measured at 873 K in air under OCV conditions. The polarization resistance of the NBSCO–*x*GDC ($x = 0$, 20, 40, and 50) composite is 0.241, 0.120, 0.105, and 0.155 cm^2 at 873 K, respectively. The ASR value is decreased with increasing the amount of

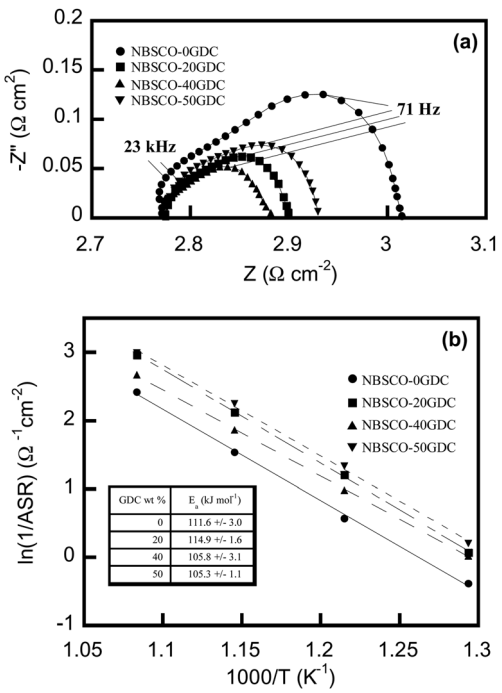

Fig. 4 (a) Typical impedance spectra of symmetric cells (NBSCO–GDC/GDC/NBSCO–GDC) measured under an open-circuit condition at 873 K in air, and (b) comparison of NBSCO–*x*GDC cathode area specific resistances plotted *versus* inverse temperature.

GDC up to 40 wt% and then starts to increase beyond 40 wt% of GDC. The electrochemical characteristics of the NBSCO–GDC composites indicate that GDC plays a significant role in improving the performance of the cathode. The observed higher catalytic activity of the NBSCO–GDC composite cathode compared to pure NBSCO might be due to the extended TPB sites with the addition of GDC, resulting in lower polarization loss of the electrodes.[17] In other words, the lower polarization of the composites can be explained on the basis of the ability of ceria based oxides to store, release, and transport oxygen under SOFC operating conditions.[33] Meanwhile, the ASR value tends to increase with excessive GDC amounts, for example, above 40 wt% in this case. It appears that the inclusion of an overly large amount of GDC particles reduces the continuity of NBSCO in the composite, thereby resulting in a decrease of effective electron-conducting paths in the electrode.

Fig. 4b shows Arrhenius plots of the polarization resistance of NBSCO–*x*GDC ($x = 0$, 20, 40, and 50) composite cathodes at various temperatures. The activation energy of NBSCO–40GDC composites, 105.7 kJ mol^{-1}, is lower than that of pure NBSCO, 111.6 kJ mol^{-1}. The errors associated with the estimation of the activation energies are listed in the table in Fig. 4b. The addition of GDC appears to reduce the activation energy of the composite compared with pure NBSCO, as the corresponding activation energy of GDC is found to be 66.57 kJ mol^{-1}. The lower activation energy of the composite cathode, at least in part, accounts for the faster oxygen diffusion process.[34,35]

Many researchers have noted that a composite cathode exhibits advanced electrochemical properties compared with a pure cathode, because the composite offers the electrochemical properties of the pure MIEC bulk as well as the electrocatalytic and ionic conducting effects from the GDC bulk;[16,36,37] this is known as the "composite effect". However, it is worth mentioning that the ASR of NBSCO–GDC composite is not improved significantly compared to that of the pure NBSCO cathode, where the composite ASR is half that of the pure cathode ASR. In contrast, Leng and Xia groups reported that a composite system provided considerable improvement in ASR compared to a pure cathode, as shown in Table 1. For example, at 873 K, a $La_{0.6}Sr_{0.4}Co_{0.2}Fe_{0.8}O_3$ composite with 60 wt% of GDC yielded an ASR of 0.17 cm^2 (ref. 36) and a $Sm_{0.5}Sr_{0.5}CoO_3$ composite with 30 wt% of $Sm_{0.2}Ce_{0.8}O_{1.9}$ showed a value of 0.18 cm^2,[38] reflecting decreases of more than ten-fold compared with the ASRs of pure cathodes. It is anticipated that, for a NBSCO–GDC composite, the ionic conductivity of GDC might not lend a significant contribution in terms of increasing performance, because the ionic conductivity of NBSCO can be considered sufficiently high for ion bulk diffusion to provide superior performance. Some double perovskite materials have shown higher oxide-ion conductivities compared with ceria based materials. For example, Taskin *et al.* reported that the ionic conductivity of an ordered double perovskite is as high as 0.01 S cm^{-1} at 773 K;[10] this value is slightly higher or comparable with that of GDC (0.0045 S cm^{-1}) at the same temperature.[39] In this NBSCO–GDC composite system, therefore, the favorable electrochemical characteristics might result from the 2PB sites of the NBSCO as well as the electrocatalytic effect at the TPB sites produced within the NBSCO–GDC composite cathode. As a result, the 40 wt% GDC composite cathode appears to be optimized for higher electrochemical performance through a combination of the favorable electrochemical properties of NBSCO as a MIEC and the high electrocatalytic characteristics of GDC.

Table 1 ASR values of the composite system at 873 K

	Pure cathode	Composite cathode
$NdBa_{0.5}Sr_{0.5}Co_2O_{5+\delta}$–GDC	0.241 Ω cm^2	0.105 Ω cm^2 (40 wt% GDC)
$La_{0.6}Sr_{0.4}Co_{0.2}Fe_{0.8}O_3$–GDC[36]	1.2 Ω cm^2	0.17 Ω cm^2 (60 wt% GDC)
$Sm_{0.5}Sr_{0.5}CoO_3$–$Sm_{0.2}Ce_{0.8}O_{1.9}$(SDC)[38]	2.5 Ω cm^2	0.18 Ω cm^2 (30 wt% SDC)

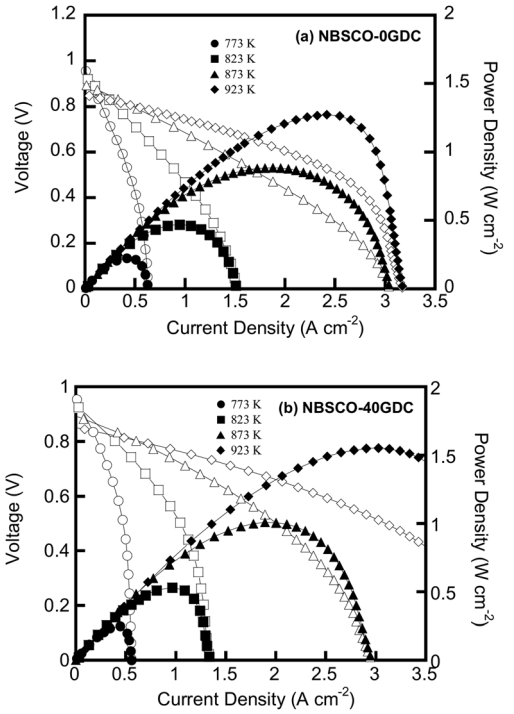

Fig. 5 Single cell performance of a cell with a $NdBa_{0.5}Sr_{0.5}Co_2O_{5+d}$–*x*GDC cathode at various temperatures; (a) NBSCO–0GDC cathode and (b) NBSCO–40GDC cathode (●; 773 K, ■; 823 K, ▲; 873 K, ◆; 923 K).

Fig. 5 shows the power density and voltage as a function of the current density for the NBSCO–GDC/GDC/Ni-GDC anode supported cell using humidified H_2 (3% H_2O) as a fuel and static ambient air as an oxidant in a temperature range of 773–923 K. The maximum power densities of the cell with the NBSCO–*x*GDC ($x = 0$, and 40) cathode materials were 0.885 and 1.086 W cm^{-2} at 873 K, respectively. The highest cell performance is achieved by the 40 wt% GDC composite cathode, which can be predicted on the basis of it having the lowest ASR. In other words, the sufficient 2PB and enhanced TPB of the composite result in the highest ORR rate, as shown in Fig. 1c, thereby providing high power density.

Conclusions

The electrochemical properties of $NdBa_{0.5}Sr_{0.5}Co_2O_{5+\delta}$–$x$$Ce_{0.9}Gd_{0.1}O_{1.95}$ cathode materials were investigated to optimize the GDC ratio for a high performance cathode for IT-SOFC application.

The XRD patterns show that both the NBSCO and the NBSCO–GDC cathodes are chemically stable under IT-SOFC operating conditions. SEM images show that the small-spherical GDC particles on the NBSCO bulk backbone enhance the sites for the oxygen reduction reaction. It is determined that GDC affects the electrochemical properties in the NBSCO–GDC composite system. For the NBSCO–GDC composite, however, the ionic conductivity of GDC might not lend a significant contribution in terms of increasing performance, because the ionic conductivity of NBSCO can be considered sufficiently high for ion bulk diffusion to provide superior performance.

The favourable electrochemical characteristics of NBSCO–GDC composites might originate from the 2PB sites of the NBSCO as well as the electrocatalytic effect at the TPB sites produced within the NBSCO–GDC composite cathode, which yields a high power density of 1.086 W cm^{-2} at 873 K. These results demonstrate that a NBSCO composite with 40 wt% GDC is an optimum cathode material for IT-SOFCs.

Acknowledgements

This research was supported by the WCU (World Class University) program (R31-2009-000-20012-0), the Basic Research Program (2012-R1A1A1013380), Mid-career Researcher Programs (2011-0010773) through the National Research Foundation of Korea funded by the Ministry of Education, Science and Technology, and the New & Renewable Energy of the Korea Institute of Energy Technology Evaluation and Planning (KETEP) grant (20113020030060) funded by the Korea government Ministry of Knowledge Economy.

References

1 Z. Shao and S. M. Haile, *Nature*, 2004, **431**, 170.
2 T. Tsai, E. Perry and S. Barnett, *J. Electrochem. Soc.*, 1997, **144**, L130.
3 S. Yoo, J. Y. Shin and G. Kim, *J. Mater. Chem.*, 2011, **21**, 439.
4 T. V. Aksenova, L. Y. Gavrilova, A. A. Yaremchenko, V. A. Cherepanov and V. V. Kharton, *Mater. Res. Bull.*, 2010, **45**, 1288.
5 K. Zhang, L. Ge, R. Ran, Z. Shao and S. Liu, *Acta Mater.*, 2008, **56**, 4876.
6 J. H. Kim, F. Prada and A. Manthiram, *J. Electrochem. Soc.*, 2008, **155**, B1023.
7 I. O. Troyanchuk, N. V. Kasper and D. D. Khalyavin, *Phys. Rev. B: Condens. Matter Mater. Phys.*, 1998, **58**, 2418.
8 J.-H. Kim and A. Manthiram, *J. Electrochem. Soc.*, 2008, **155**, B385.
9 G. Kim, S. Wang, A. J. Jacobson, L. Reimus, P. Brodersen and C. A. Mims, *J. Mater. Chem.*, 2007, **17**, 2500.
10 A. A. Taskin, A. N. Lavrov and Y. Ando, *Appl. Phys. Lett.*, 2005, **86**, 091910.
11 J. H. Kim, M. Cassidy, J. T. S. Irvine and J. M. Bae, *J. Electrochem. Soc.*, 2009, **156**, B682.
12 H. Ding and X. Xue, *Electrochim. Acta*, 2010, **55**, 3812.
13 H. Kozuka and K. Yamagiwa, *J. Mater. Chem.*, 2012, **22**, 11003.
14 T. He, J. Chen, T. G. Calvarese and M. A. Subramanian, *Solid State Sci.*, 2006, **8**, 467.
15 C. R. Dyck, Z. B. Yu and V. D. Krstic, *Solid State Ionics*, 2004, **171**, 17.
16 V. Dusastre and J. A. Kilner, *Solid State Ionics*, 1999, **126**, 163.
17 Q. Zhou, W. Wang, T. Wei, X. Qi, Y. Li, Y. Zou, Y. Liu, Z. Li and Y. Wu, *Ceram. Int.*, 2010, **38**, 1529.
18 S. B. Adler, *Chem. Rev.*, 2004, **104**, 4791.
19 J. A. Lane, S. J. Benson, D. Waller and J. A. Kilner, *Solid State Ionics*, 1999, **121**, 201.
20 S. J. Skinner, *Int. J. Inorg. Mater.*, 2001, **3**, 113.
21 O. Yamamoto, Y. Takeda, R. Kanno and Y. Tomida, *Nippon Kagaku Kaishi*, 1998, **8**, 1324.
22 M. Gödickemeier, K. Sasaki, L. J. Gauckler and I. Riess, *Solid State Ionics*, 1996, **86–88**, 691.
23 J. A. Lane, S. B. Adler, P. H. Middleton and B. C. H. Steele, *Solid Oxide Fuel Cells (SOFC-IV)*, 1995, pp. 584–596.
24 E. Maguire, B. Gharbage, F. M. B. Marques and J. A. Labrincha, *Solid State Ionics*, 2000, **127**, 329.
25 B. Rohland, *Mater. Sci. Forum*, 1991, **76**, 149.
26 T. Takahashi, M. Ihara and K. Yamada, *Development of SOFC Cathodes for Reduced-Temperature Applications, Proceeding of the Fourth International Symposium on Solid Oxide Fuel Cell*, 1995, pp. 1009–1017.
27 M. T. Colomer, B. C. H. Steele and J. A. Kilner, *Solid State Ionics*, 2002, **147**, 41.
28 B. C. H. Steele, *Solid State Ionics*, 1997, **94**, 239.
29 W. Schäfer, A. Koch, U. Herold-Schmidt and D. Stolten, *Solid State Ionics*, 1996, **86–88**, 1235.
30 A. Endo, H. Fukunaga, C. Wen and K. Yamada, *Solid State Ionics*, 2000, **135**, 353.
31 S. B. Adler, *Solid State Ionics*, 1998, **111**, 125.
32 J. H. Kim and J. T. S. Irvine, *Int. J. Hydrogen Energy*, 2012, **37**, 5920.
33 M. Mogensen, N. M. Sammes and G. A. Tompsett, *Solid State Ionics*, 2000, **129**, 63.
34 Z. Zhan, D. Han, T. Wu, X. Ye, S. Wang, T. Wen, S. Cho and S. A. Barnett, *RSC Adv.*, 2012, **2**, 4075.
35 S.-H. Park and H.-I. Yoo, *Solid State Ionics*, 2005, **176**, 1486.
36 Y. Leng, S. H. Chan and Q. Liu, *Int. J. Hydrogen Energy*, 2008, **33**, 3808.
37 S. J. Lee, D. S. Kim and D. K. Kim, *Curr. Appl. Phys.*, 2011, **11**, S238.
38 C. Xia, W. Rauch, F. Chen and M. Liu, *Solid State Ionics*, 2002, **149**, 11.
39 Q. X. Fu, W. Zhang, R. R. Peng, D. K. Peng, G. Y. Meng and B. Zhu, *Mater. Lett.*, 2002, **53**, 186.